Nanoscale

Accepted Manuscript

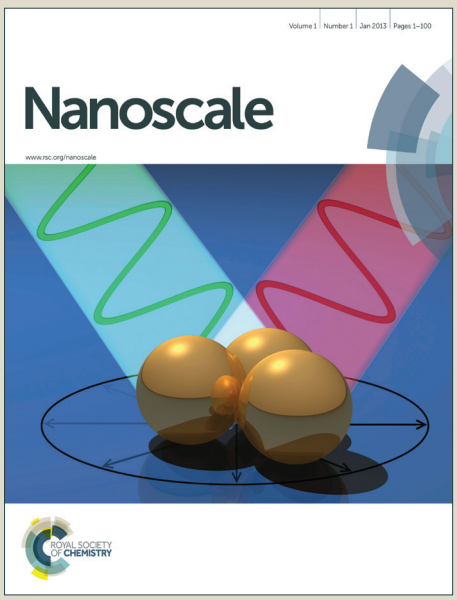

ROYAL SOCIETY OF CHEMISTRY

www.rsc.org/nanoscale

Journal Name

RSCPublishing

ARTICLE

Small molecule BHJ solar cells based on DPP(TBFu)$_2$ and diphenylmethanofullerenes (DPM): Linking morphology, transport, recombination and crystallinity

Cite this: DOI: 10.1039/x0xx00000x

Received ooth January 2012,
Accepted ooth January 2012

DOI: 10.1039/x0xx00000x

www.rsc.org/

Daniel Fernández,[a] Aurélien Viterisi,[a] James William Ryan,[a] Francesc Gispert-Guirado,[b] Sara Vidal,[c] Salvatore Filipone,[c] Nazario Martín,[c]* and Emilio Palomares[a]*

The effect of alkyl chains in substituted diphenylmethano[70]fullerenes (C70-DPM) on the device characteristics of DPP(TBFu)$_2$ small molecule-based bulk heterojunction (BHJ) organic solar cell devices are investigated. By measuring charge carrier mobilities as well as the morphology and crystallinity of each device we have been able to explain and understand the differences found between solar cells made with the different C70-DPM fullerenes despite the general lack of simple relationships between molecular structure, orbital level positioning and power conversion efficiency. Our study then concludes with some general rules for the future design of acceptors for DPP(TBFu)$_2$ containing photoactive layers in the search for efficient organic solar cells.

Introduction

The field of solution processed bulk-heterojunction (BHJ) solar cells has been widely dominated by polymer or small molecule donors and fullerene-based acceptors.[1] Of these fullerene acceptors, the phenyl-butyric acid methyl ester substituted series ($PC_{60}BM$ and $PC_{70}BM$) have been by far the most commonly used. However, the ease of functionalization of the fullerene core has driven the search for new alternatives as the fullerene properties can be easily tuned by varying the functional groups while retaining the core's electronic properties. Particularly, it is well known that solubility, processability and HOMO-LUMO level positioning can be tuned by adequate chemical functionalization. Numerous alternatives have been published to date,[2] but surprisingly only few structures have given better power conversion efficiencies (PCEs) than devices made with their methyl esters counterparts.[2a,3] These new acceptors have shown to have a strong effect on the crystallization process of the donor polymer domains, in polymer-based OSC devices, and can in some cases significantly impair device function.[4]

A diphenylmethano[60]fullerene (C_{60}-DPM) derivative bearing two lateral C_{12} aliphatic chains has previously been studied by others[5] and us in polymer-based devices.[4b] Although the experimental HOMO-LUMO levels of this new fullerene derivative where essentially similar to those of $PC_{60}BM$, it was shown to induce some distinct changes in the device performance. These properties were explained by the fact that C_{60}-DPM12 affects the crystallinity of the P3HT donor domains. [4b, 5b] Similarly to polymer-based solar cells, the properties of SM-BHJ OSC have shown to be dependent on the crystallinity of the donor domains, and probably to a much greater extent. It has been demonstrated that in such type of devices crystalline growth of donor domains is either promoted or impeded depending on the type of fullerene derivative used in the active layer blend.[6] The crystallite's growth seems to be related to the ratio of aliphatic over the aromatic carbons of the fullerene derivative, so that an optimum size of alkyl chain is required to promote donor's crystallite growth.[6a]

Based on our previous work on the use of solvent annealing to control the thin film nanomorphology [6b] we describe herein the preparation of solar cells devices based on a small molecule DPP(TBFu)$_2$ donor and a series of C70-DPM fullerene derivatives bearing alkyl chains of a different length, varying from 4, 6 to 12 carbons (**Figure 1**) with the aim to learn more about the relation between nanocrystalline domains in the photo-active layer and the device performance under working conditions. The presence of alkyl chains in the fullerene is expected to promote changes on the thin film nanomorphology that may also induce changes on (a) device performance and (b)

charge transfer reactions at the materials interface. We have carried out a thorough characterization of the devices, in order to understand how the effect of fullerene substitution impacts the crystallinity and how this change in crystallinity is influencing the electronic transport and recombination properties of the devices.

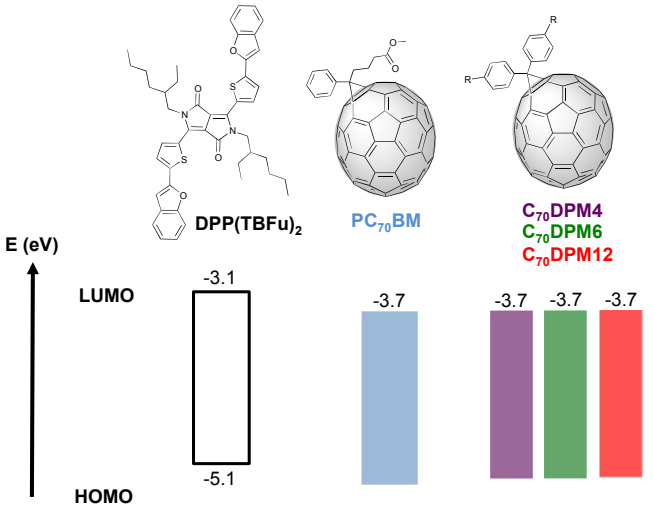

Figure 1. Molecular structure of the DPP(TBFu)$_2$ donor and the C$_{70}$-DPM series of fullerene used in the study, with their experimental HOMO and LUMO levels derived from cyclic voltametry and UV-Visible/steady-state emission measurements.

The effect of the different C$_{70}$-DPM fullerenes on the crystallinity of the donor domains has been investigated both quantitatively and qualitatively using 1D and 2D X-Ray diffraction on active layers films. Space Charge Limited Current (SCLC) electron and hole charge carrier mobilities were measured on devices made from the different C$_{70}$-DPM derivatives. Transient absorption spectroscopy (TAS) on active layer films and charge carrier recombination measurements carried out on complete devices using the transient photocurrent/transient photovoltage technique (CE/TPV) combined with ideality factor analysis provided insights on difference in band structure and energetic defects brought about by the C$_{70}$-DPM series with respect to the PC$_{70}$BM acceptor.

Results and discussion

The crystallinity of donor domains in SM-BHJ devices has shown to be of capital importance to obtain good devices characteristics. In a previous study from our group we demonstrated that crystallite growth was very significantly enhanced in active layer blends of DPP(TBFu)$_2$:PC$_{70}$BM compared to films of pristine DPP(TBFu)$_2$ SM donor. The enhancement of crystallite growth then attributed to the presence of PC$_{70}$BM in the blend motivated us to investigate on the influence of fullerene functionalization on crystal growth of donor domains in SM-BHJ devices. To do so we employed a well-known structure depicted in **Figure 2**, where the active layers consisted of blend of DPP(TBFu)$_2$ and three different fullerene derivatives to which solvent annealing (with CH_2Cl_2) was applied as a post-deposition treatment. Such treatment has shown to promote crystal growth in active layers made out of small molecule:fullerene blends , particularly in devices using the DPM's fullerenes.

Prior to study the crystallinity of the different blends devices were fabricated with each C$_{70}$-DPM derivative and PC$_{70}$BM for reference purposes, and optimised for donor/acceptor (D/A) ratio, active layer thickness and annealing time. This provided a broad trend in the *J-V* characteristics, where both FF and J_{SC} are seen to decrease relative to the alkyl chain length of the fullerene (**Figure 2**).

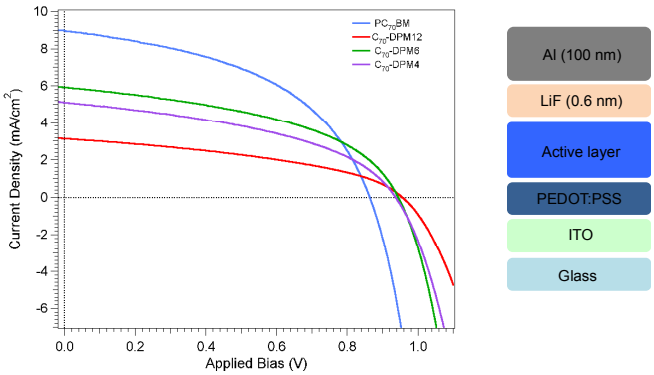

Figure 2. *J-V* characteristics of solar cell devices fabricated with PC$_{70}$BM and the C$_{70}$-DPM series acceptors. These curves represent the average performance of devices made under optimized conditions.

The V_{OC} is however consistently higher in devices made from the C$_{70}$-DPM fullerenes (**Table 1**).

Table 1: Device parameters (area 9mm^2) under 100mW/cm^2 sun simulated irradiation with active layers made with C70-DPM fullerene series and PC$_{70}$BM. The active layer thickness was 80nm±10nm.

Fullerene derivative	V_{OC}	J_{SC}	FF	PCE (%)
PC$_{70}$BM	0.858	8.97	48	3.64
C$_{70}$-DPM4	0.933	5.10	43	2.06
C$_{70}$-DPM6	0.944	5.92	45	2.55
C$_{70}$-DPM12	0.954	3.13	40	1.21

The physics underpinning such feature will be explained below. The decrease in J_{SC} is corroborated by IPCE measurements showing a decrease in the overall IPCE value (**Figure 3b**) over the all range of the visible region.

The change in the UV-Vis absorption measured (**Figure 3a**) in active layers prepared using conditions of optimised devices follows a previously described trend where the appearance of blue shifted absorption bands typical of aggregation features is observed in all cases.[6b, 7] The slight variation in the intensity of the bands is attributed to the slight difference in device thickness and D/A ratio in the blends.

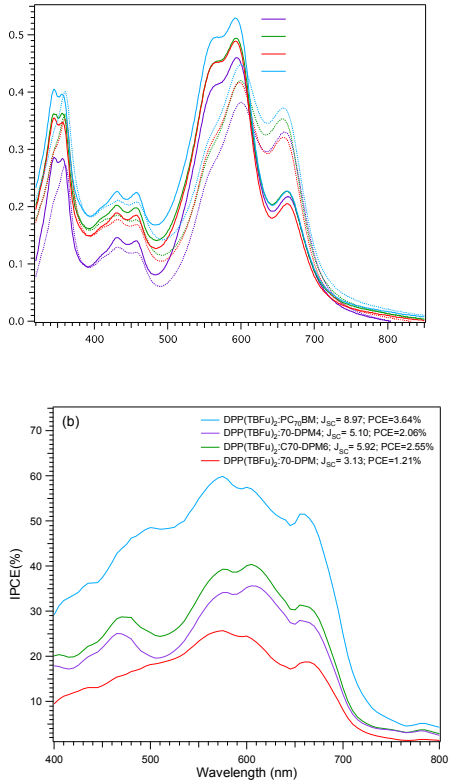

Figure 3. a) UV-Visible absorption spectra of CH_2Cl_2 solvent-annealed (solid line) and non-annealed (dotted line) DPP(TBFu)$_2$:fullerene active layers films. b) IPCE curves of solar cell devices whose *J-V* characteristics are shown in **Figure 2**.

This aggregation characteristic in the solid state had been related to a crystallization process and well characterised using XRD experiments.[6b] Similarly, we first utilised out-of-plane grazing incidence XRD (GIXRD) setup with area detector to obtain qualitative information on the orientation of crystallites of donor in the active layer. Subsequent measurements with a point detector in reflection mode allowed for a quantitative analysis. The area detector images taken from active layers prepared on glass substrates in the same conditions as optimised devices, are in agreement with previously reported results, with the appearance of a diffraction spot upon annealing in all active layers at 2θ=6.1° with interplanar spacing of 14.5 Å attributed to crystalline domains of the donor material (**Figure 4**).[6b, 7] The texture in the annealed films shows a rather similar trend as in the reference DPP(TBFu)$_2$:PC_{70}BM where the crystallites adopt a rather homogenous orientation. However, the appearance of additional well resolved Debye rings superimposed on the main diffraction spot in the case of C_{70}-DPM6 and C_{70}-DPM12 active layer is strong evidence for the presence of two different populations of crystallites, one very well oriented (along the out-of-plane direction) and the other randomly oriented.

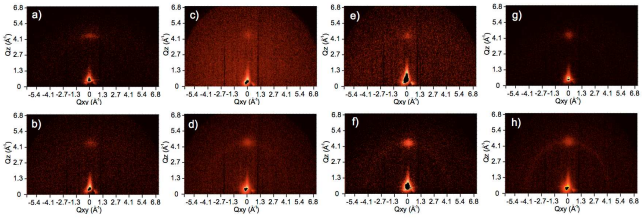

Figure 4. Area detector image in the out-of-plane direction of non annealed and solvent annealed films of a) and b) DPP(TBFu)$_2$:PC_{70}BM blend (t_a= 60 sec.) c) and d) DPP(TBFu)$_2$:C_{70}-DPM4 blend (t_a= 60 sec.) e) and f) DPP(TBFu)$_2$:C_{70}-DPM6 blend (t_a= 60 sec.) g) and h) DPP(TBFu)$_2$:C_{70}-DPM12 blend (t_a= 60 sec.) obtained in reflexion mode with an incident angle of ω=0.5° at a distance of 30 cm.

The point detector diffractograms (**Figure 5**) confirm the crystalline growth triggered by SVA, and, using the diffraction peak parameters such as the FWHM and integrated area an approximate relative quantification was possible. However due to the out-of-plane set up limitation only the fraction of oriented crystallites could be quantified. Out of that fraction the data show that the largest crystallites of donor grow when PC_{70}BM is part of the blend and the crystallite size decreases upon increasing the alkyl chain length in the case of C_{70}-DPM fullerenes. It appears that crystalline growth is very much limited in the C_{70}-DPM-based devices and crystallite size remains in the range of those of pristine DPP(TBFu)$_2$ films[6b] as seen by the values of FWHM in **Figure 5**. The integrated area of the diffraction peaks accounts for a larger fraction of crystalline material in the active layers of C_{70}-DPM4 and DMP6 relative to PC_{70}BM, where the integrated area is greater for C_{70}-DPM4 and C_{70}-DPM6 while the lowest value is seen for C_{70}-DPM12.

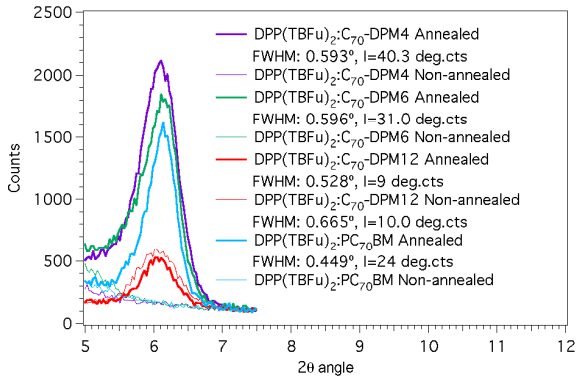

Figure 5. Point detector diffractograms of annealed and non-annealed active layers taken in reflexion mode. The peak parameters are reported in the legend.

The AFM images of un-annealed and annealed devices **(Figure 6)** corroborate the crystallisation process characterised by X-ray diffraction, nonetheless some striking differences were seen between the fullerene blends studied. The active layers of C_{70}-DPM6 and $PC_{70}BM$ fullerenes display a rather flat morphology with smooth surface when un-annealed as seen by the RMS roughness value, while those of C_{70}-DPM4 and C_{70}-DPM12 display very large 'aggregate-like' features giving rise to much higher roughness values. Interestingly, all layers rearrange to a very similar morphology upon SVA, with roughness value in the same range for all active layers, showing the effect of SVA in providing thermodynamic freedom by locally dissolving molecules and allowing them to rearrange at the nanoscale.[8]

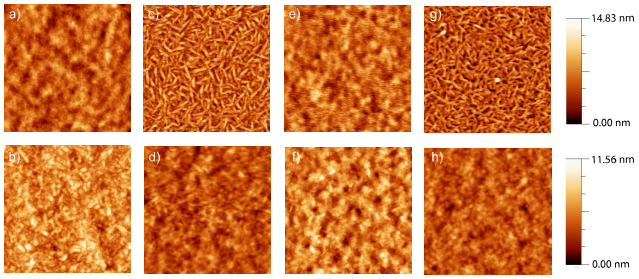

Figure 6. 2D AFM micrographs non annealed (5×5 µm) and solvent annealed (2×2 µm) films of a) and b) DPP(TBFu)$_2$:$PC_{70}BM$ blend (t_a= 60 sec.) c) and d) DPP(TBFu)$_2$:C_{70}-DPM4 blend (t_a= 60 sec.) e) and f) DPP(TBFu)$_2$:C_{70}-DPM6 blend (t_a= 60 sec.) g) and h) DPP(TBFu)$_2$:C_{70}-DPM12 blend (t_a= 60 sec.).

The formation of large domains in C_{70}-DPM4 and C_{70}-DPM12 films before the annealing process (**Figure 6 c) and g**)) may stem from the high level of incompatibility between the donor and these two acceptors. A presumably strong repulsion interaction in solution between these fullerenes and the donor molecule could lead to a strong segregation upon the fast drying conditions of the spin coating processing of the active layer. Subsequently when the active layers are submitted to SVA, thermodynamic freedom is brought to the system for it to equilibrate in such a manner that the interface energy lowers leading to a more or less rapid growth of crystalline donor domains limited by the magnitude of the interactions between the different materials at their interface. Analogously to crystalline growth on a macroscopic scale, the surface energy of the crystallites is believed to increase proportionally to the rate of crystallite growth and will eventually define the size of the final crystallites. In the case of the active layers studied herein the surface energy is believed to be directly related to the crystallite/amorphous-material[9] interaction, thus explaining the difference in crystallinity of the active layers made with the different fullerene derivatives. Varying the SV annealing time supposedly allows trapping the morphology in this equilibration path, affording active layers with different crystallite size and different crystalline volume as previously demonstrated. It is likely that the solvent in the SVA step merely acts as a 'catalyst' lowering the activation energy of the process, which would otherwise happen on a much slower time scale. Such hypothesis is supported by the fact that some of the active layers made with C_{70}-DPM derivatives show a tendency to 'self-anneal', whereby a non-annealed film of the active layer undergoes a colour change consistent with crystalline growth within a mater of hours. Thus the faint diffraction peaks observed in non-annealed films in **Figure 4** (picture c, e, g) are simply arising from this 'self-annealing' process. Those peaks are not observed in the point detector diffractogram as this data could be acquired just a few hours after active layer deposition. For the case of C_{70}-DPM12-based active layer the diffraction peak appears in the point detector data of the un-annealed film as the kinetics of self-annealing at room temperature are much faster than for the active layers of other fullerenes (See Supporting Information).

As previously demonstrated, the crystallinity features explained above (Figure 4 and Figure 6) are reflected in the device's characteristics. Additionally, the difference in crystallinity of the active layer has a significant impact on the D/A interface and thus on polaron pair generation and recombination.

Transient absorption spectroscopy provides for a practical method to approximately quantify the generation yield of polaron pairs that have escaped the CT coulombic attraction. By comparing the amplitude of the decay transients of the different active layers where the laser pulse is held at a constant distance from the substrate and at constant intensity one can obtain valuable information of the efficiency of the overall charge generation process since the magnitude of the polaron light absorption is proportional to the density of generated polarons in the blend film.[10] Therefore, TAS was measured on samples of DPP(TBFu)$_2$:fullerene blends deposited on glass substrates and annealed in a vapour of CH_2Cl_2 similarly to optimised devices. The films were excited with an incident laser pulse with wavelength of 580 nm and the transients recorded at a wavelength of 990 nm the absorption maximum of the DPP(TBFu)$_2$ polaron absorption band (see Supporting Information), determined from the reference sample of DPP(TBFu)$_2$:$PC_{70}BM$ active layer film. Interestingly the

decays of all blend film show strong similarities in both, amplitude of the signal and decay life-time, the slight difference in signal intensity being attributed to the slight difference in absorption of the films (see **Figure 7**). Therefore the data suggests a similar polaron generation yield.

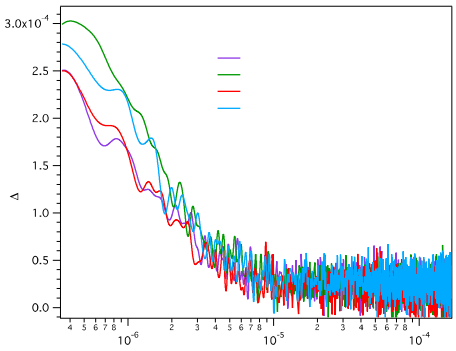

Figure 7. Photo-induced laser transient absorption decays of DPP(TBFu)$_2$:fullerene films. Laser excitation wavelength was set at 580 nm and decays were registered at λprobe = 990nm

It should be noted, however, that the generation yield measured in blend films from the TAS measurement does not take into account the presence of electrodes as in complete devices, which could potentially contribute to the CT (charge transfer) separation yield. In the present case the structure of the complete devices being similar and varying only from their active layers, the effect of the electrodes is expected to have a similar contribution on the CT separation yield in all the devices and thus are not expected to induce any change in the relative overall free polaron pair generation in devices. Consequently, since a similar density of free polaron pairs are generated in all devices it could be assumed the differences in the devices' characteristics, particularly J_{SC}, is likely to be principally left to charge collection properties.

To address this issue, space charge limited current (SCLC) hole and electron carrier mobilities were measured on all devices. Hole and electron only devices, were fabricated according to standard reported procedures, and the SCLC region was recorded by sweeping the forward bias to large values of potential (see SI). Hole and electron SCLC could not be fitted to the conventional Mott-Gurney equation, nonetheless it was fitted to a field dependent equation.[11] **Table 2** shows that the values of the zero field mobilities, from which electron mobilities for DPM-based acceptor are in good agreement with values reported for polymer and small molecule blends.[7, 12]

Table 2: Hole and electron mobility values for devices with active layers made with C70-DPM fullerene series and $PC_{70}BM$.

Fullerene derivative	μ hole	μ electron
$PC_{70}BM$	1.2×10^{-5}	0.8×10^{-3}
C_{70}-DPM4	0.6×10^{-6}	4.6×10^{-6}
C_{70}-DPM6	1.5×10^{-5}	3.4×10^{-5}
C_{70}-DPM12	2.2×10^{-8}	2.8×10^{-7}

Electron mobility is seen to be higher for devices made using C_{70}-DPM6 and $PC_{70}BM$ while the value decreases significantly for devices C_{70}-DPM4 and C_{70}-DPM12. The mobility results also show an important difference between the C_{70}-DPM4 and C_{70}-DPM12 fullerenes as in the case of C_{70}-DPM4 only hole mobility is slightly reduced while in the case of C_{70}-DPM12 both hole and electron mobilities are of lower magnitude. The hole mobility of C_{70}-DPM6 and $PC_{70}BM$ have a very similar value, showing that the limiting factor in the case of C_{70}-DPM6 appears to be solely electron mobility. It seems clear from these results that the drop in performance of devices made with C_{70}-DPM fullerene derivatives is partly explained by a difference in crystalline size and crystalline volume of the donor's material domains inducing a change in hole mobility, but also –equally as important– by a decrease in electron mobility inherent to the functionalization of the fullerene derivative. Therefore, although the active layer incorporating C_{70}-DPM4 and C_{70}-DPM6 fullerenes account for a higher volume of donor's crystallites respect to DPP(TBFu)$_2$:$PC_{70}BM$, and that polaron pair generation is of similar magnitude, J_{SC} remains below that of devices incorporating $PC_{70}BM$ in their active layer, in agreement with the lower electron mobilities measured for C_{70}-DPM4 and C_{70}-DPM6.

Now we turn on to the study of the V_{OC}, which origin is generally thought of being proportional to the difference between the LUMO energy level of the acceptor and the HOMO level of the donor. However, in the present case the LUMO level of the fullerene are not shown to vary with chemical functionalization and the experimental difference in V_{OC} between the different devices is more likely to be determined by recombination kinetics.[13] In order to identify how the latter contributes to V_{OC} and to some extent to the shape of the *J-V* characteristics, a qualitative recombination study was carried out using a well-established charge extraction and transient photovoltage method (see SI for experimental details).[13a, 14] The CE measurements allow measuring the average charge density at open circuit in the devices. **Figure 8a** shows the plot of the charge density (*n*) *vs.* open circuit voltage obtained from CE for the all devices where *n* was corrected for the electrode capacitance (see SI). The data shows to be in good agreement with the charge density being of similar magnitude in all measurements, reaching about 2×10^{16} charges/cm^3 at values close to V_{OC} similarly to what has been

reported earlier for such type of devices.[13a, 14i] In all the devices the total charge is seen to increase almost linearly with V_{OC} up to a certain value where the variation becomes exponential a feature that has been observed earlier in SM BHJ and SM bilayer devices linked with the extreme thinness of the active layer respect to polymer based devices.[13a, 14g, 14i, 15] Nonetheless, the exponential variation over the higher values of charge density (greater light bias) is evidence of charges accumulated in the bulk of the device.

Table 2: Values of recombination parameters derived from CE/TPV measurements for devices with active layers made with C_{70}-DPM fullerene series and $PC_{70}BM$.

Fullerene derivative	n_0	γ	β	λ	□
PC70BM	7.5×10^{14}	3.5	22.9	7.4	8.4
C70-DPM4	4.5×10^{14}	3.8	21.7	5.4	6.4
C70-DPM6	4.8×10^{14}	3.7	20.9	5.4	6.4
C70-DPM12	2.6×10^{14}	4.2	19.7	4.7	5.7

The plots of *n vs.* V_{OC} were fitted to single exponentials of the form of **Equation 1**, analogously to the splitting of the quasi-Fermi levels in intrinsic semiconductors, where the value of γ (from ≈3.8V^{-1} for DPP(TBFu)$_2$:DPM4 to ≈4.2 V^{-1} for DPP(TBFu)$_2$:C_{70}-DPM12, see **Table 2**) is lower than that expected for ideal semiconductors, an effect that has been attributed to the presence of an exponential tail of trap states extending into the band gap of the active layer.[16]

$$n = n_0 e^{\gamma Voc} \qquad \textbf{Equation 1}$$

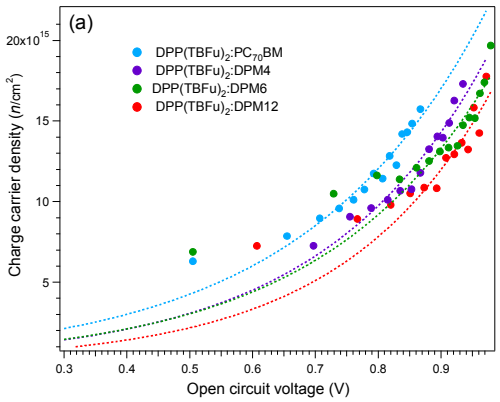

$$\tau_{\Delta n} = \tau_0 e^{-\beta Voc} \qquad \textbf{Equation}$$

The carriers life time ($\tau_{\Delta n}$) versus open circuit voltage (V_{OC}) plot for all the devices is shown in **Figure bb**, where the curves were fitted to single exponential decays of the form of **Equation 2**.

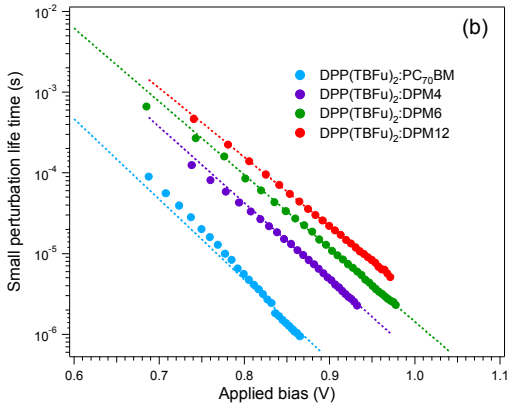

Figure 8. a) Comparison of the charge density (*n*) as a function of the open circuit voltage determined from CE measurement. The curves are fitted to an exponential grow of the form $n=n_0e^{(\gamma VOC)}$ (dotted line) whose parameters are reported in **Table 2**. b) Carriers lifetime measured using TPV as a function of device open circuit voltage. The curves are fitted to an exponential decay of the form $\tau_{\Delta n}=\tau_{\Delta n0}e^{(-\beta VOC)}$ (dotted line) whose parameters are reported in **Table 2**.

The plots in **Figure 8a** and **Figure 8b** were combined as shown in **Figure 9a** and used to determine the overall order of recombination □, defined by **Equation 3**, which can be approximated to □ = λ+1, in our TPV experimental conditions ($\Delta n<<n$).[14h] The parameter λ is obtained experimentally by fitting the curve of the small perturbation carrier life time $\tau_{\Delta n}$ *vs*. *n* to a power law of the form of **Equation 4**.

$$\frac{dn}{dt} = -kn^{\phi} \qquad \textbf{Equation 3}$$

$$\tau_{\Delta n} = \tau_{\Delta n0} n^{-\lambda} \qquad \textbf{Equation 4}$$

Interestingly the recombination order varies significantly from device to device, with unexpectedly high values (ϕ = 8.4) for the devices displaying lower V_{OC}. Such high values, as opposed to a value of 2, which is to be expected in a strictly bimolecular recombination process in the case of Langevin type recombination, have been measured several times in earlier reports,[14h, 16c, 16d, 17] and were attributed to recombination through trap states in the band gap of the active layer materials.[17] Therefore the non-geminate recombination process is described as an essentially bimolecular process where the recombination coefficient is allowed to be charge dependent

accordingly to the presence of trap states in the band gap.[14c, 14e, 14h]

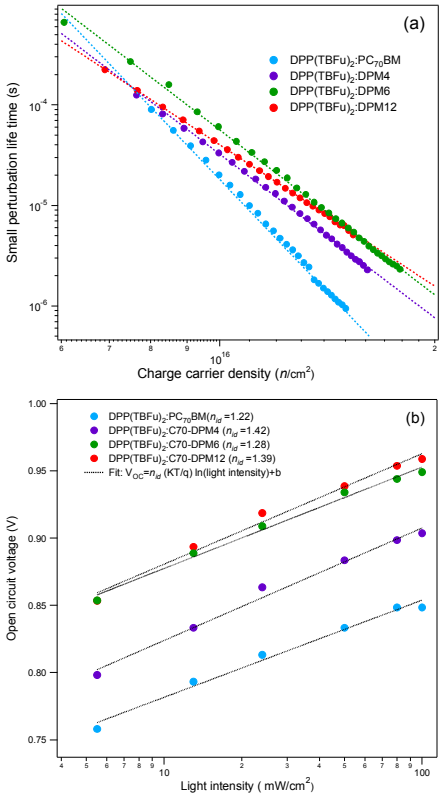

Figure 9. a) Small perturbation carrier life time vs. open circuit voltage plot for devices made with the C_{70}-DPM series and reference DPP(TBFu)2:$PC_{70}BM$ blends. Curves are fitted to power law decays of the form $\tau_{\Delta n}=\tau_{\Delta n0}\, n^{-\lambda}$, whose parameters are reported in **Table 2**. b) Open circuit voltage vs light intensity for all devices used in this work.

It is interesting to note that the devices made with DPM4 and DPM6 derivatives both show a similar apparent recombination order of about 6 and that devices made with DPP(TBFu)$_2$:$PC_{70}BM$ blends have a higher recombination order (8.4). Nevertheless, the recombination life times measured through CE/TPV correspond to a total charge carrier recombination and therefore it is difficult to attribute the experimental reaction order (□) obtained using this method to a specific recombination mechanism. Indeed it has been showed, that, especially in thin active layers as in our case, surface recombination or doping can have a very significant influence on the apparent recombination order.[18] To gain more insight on this matter we calculated the ideality factor (n_{id}) of all devices by fitting the V_{OC} *vs.* Light bias plot to a logarithmic function as depicted in **Figure 9b**. The values of n_{id} obtained are in the range of expected value for thin devices (d<100 nm) where surface recombination is significant and where a moderate concentration of deep traps is present.[18] Given that the thickness is similar in all the devices, the lower n_{id} for the device made with $PC_{70}BM$ would then be explained by a higher mobility as observed experimentally. In the case of DPM-based devices the higher n_{id} would be consistent with a slightly higher density of deep trap states, corroborated by the lower apparent recombination order, and consistent with lower crystallinity of the active layer. Those deeper traps could be the result of the presence of a population of disorientated DPP(TBFu)$_2$ crystallites in the case of DPM-based devices (*vide supra*) creating inhomogeneous crystallites boundaries. The presence of a larger population of oriented crystallites in DPM4 and DPM6-based devices respect to the $PC_{70}BM$-based ones does not compensate for the defects brought by the ill-oriented fraction since although the total crystalline volume is greater, the crystallites are smaller in size thus generating more boundaries than in $PC_{70}BM$-based active layer.

The slopes of the n vs applied bias plots combined with the recombination lifetime follow the trend observed for the V_{OC} of the devices. That is, the devices with broader DOS (qualitatively estimated through the parameter γ in the n *vs.* applied bias plot) and faster recombination kinetics display the lowest V_{OC} as in the $PC_{70}BM$ or DPM-based devices, whereas the opposite trend is exemplified by DPP(TBFu)2:DPM12 devices. A similar trend had been observed in polymer-based OSC devices comprising C_{70}-DPM fullerene derivatives, whereby the HOMO-LUMO energy levels of the fullerenes derivatives could not explain the difference in the experimental Voc.[4b, 5b]

Conclusions

The present study has allowed the in-depth understanding of the very limiting factors of the PCE in small molecule BHJ devices based on DPP(TBFu)$_2$.

By using an extensive set of characterisation techniques we have been able to obtain important insights into the morphological changes induced by different fullerene acceptors on the active layer of DPP(TBFu)$_2$-based BHJ devices. First X-Ray diffraction and AFM have shone light on the kinetics of the crystalline growth triggered by SVA in the active layers, demonstrating that the fullerene acceptors have a strong impact on the quantity and size of crystallites of donor material formed. A broad trend could be drawn where the crystalline features decrease with longer alkyl chain functionalization of the fullerenes. Subsequently, transient absorption spectroscopy revealed that those changes in crystallinity have an apparently insignificant effect on polaron pair generation; however hole mobility was very significantly affected as measured by SCLC. Additional data on electron mobility showed that the fullerene functionalization is critical in providing high electron mobility and that excessive alkyl chain length functionalising group leads to extremely low mobilities.

Finally, data on non-geminate recombination kinetics obtained by CE/TPV methods provided important qualitative information on the variation of the band structure and the recombination kinetics of the devices incorporating the different fullerenes. Indeed, although all fullerene derivatives showed very similar LUMO levels the change in crystallinity

they cause on the donor domains and their intrinsic solid-state band properties, induce a significant change on the hole/electron averaged DOS distribution and on the non-geminate recombination order. Such changes explain the difference in V_{OC} observed experimentally. Additionally, simple ideality factor comparison between devices allowed withdrawing information on the band structure difference brought about by the different fullerenes.

All in all, this study provided important insights for the design of new fullerene-based acceptors, whereby, to provide improved devices' characteristics not only should they display the highest possible electron mobility, but as importantly, must interact with the donor in a favourable manner in order to induce the formation of large and numerous donor crystallites in the active layer. The nature of such type of weak interaction is currently being investigated in the laboratory.

Acknowledgements

We would like to thank the financial support of ICIQ and ICREA as well as the Spanish MINECO for the project CTQ2010-18859. EP wish to thanks the EU for the ERCstg PolyDot project and the Catalan regional government for the 2009 SRG 207 project. Prof. Nazario martin also would like to acknowledge the financial support by MINECO of Spain (projects CTQ2010-16959 and Consolider-Ingenio CSD2007-00010), and the Madrid regional government for the CAM (MADRISOLAR-2 project S2009/PPQ-1533).

Notes and references

[a] *Institute of Chemical Research of Catalonia (ICIQ), Av. Països Catalans, 16, Tarragona 43007, Spain.*
[b] *Universitat Rovira I Virgili, Scientific Resources Service, Avda. Països Catalans 26, 43007 Tarragona, Spain.*
[c] *Departamento de Química Orgánica, Facultad de Ciencias Químicas, Universidad Complutense, 28040 Madrid, Spain.*
** To whom correspondence should be addressed: Email: epalomares@iciq.es; nazmar@quim.ucm.es*

† Electronic Supplementary Information (ESI) available: [Devices' fabrication and characterisation, XRD measurements details, cyclic voltamograms, hole and electron mobility measurements, CE/TPV experimental details]. See DOI: 10.1039/b000000x/

1. a) C. J. Brabec, S. Gowrisanker, J. J. M. Halls, D. Laird, S. Jia and S. P. Williams, *Adv. Mater.*, 2010, **22**, 3839; b) C. Deibel and V. Dyakonov, *Rep. Prog. Phys.*, 2010, **73**, 096401; c) W. Cai, X. Gong and Y. Cao, *Sol. Energy Mater. Sol. Cells*, 2010, **94**, 114; d) H.-L. Yip and A. K. Y. Jen, *Energy Environ. Sci.*, 2012, **5**, 5994; e) P. M. Beaujuge and J. M. J. Fréchet, *J. Am. Chem. Soc.*, 2011, **133**, 20009; f) J. L. Delgado, P. A. Bouit, S. Filippone, M. A. Herranz and N. Martin, *Chem. Commun.*, 2010, **46**, 4853.

2. a) C.-Z. Li, H.-L. Yip and A. K. Y. Jen, *J. Mater. Chem.*, 2012, **22**, 4161; b) B. Walker, C. Kim and T.-Q. Nguyen, *Chem. Mater.*, 2011, **23**, 470; c) A. Mishra and P. Bäuerle, *Angew. Chem., Int. Ed.*, 2012, **51**, 2020; d) Y. Lin, Y. Li and X. Zhan, *Chem. Soc. Rev.*, 2012, **41**, 4245.

3. a) Y. He, H.-Y. Chen, J. Hou and Y. Li, *J. Am. Chem. Soc.*, 2010, **132**, 1377; b) G. Zhao, Y. He and Y. Li, *Adv. Mater.*, 2010, **22**, 4355; c) Y. He, G. Zhao, B. Peng and Y. Li, *Adv. Funct. Mater.*, 2010, **20**, 3383.

4. a) F. C. Jamieson, E. B. Domingo, T. McCarthy-Ward, M. Heeney, N. Stingelin and J. R. Durrant, *Chem. Sci.*, 2012, **3**, 485; b) A. Sánchez-Díaz, M. Izquierdo, S. Filippone, N. Martin and E. Palomares, *Adv. Funct. Mater.*, 2010, **20**, 2695; c) J. H. Choi, K.-I. Son, T. Kim, K. Kim, K. Ohkubo and S. Fukuzumi, *J. Mater. Chem.*, 2010, **20**, 475.

5. a) I. Riedel, E. von Hauff, J. Parisi, N. Martín, F. Giacalone and V. Dyakonov, *Adv. Funct. Mater.*, 2005, **15**, 1979; b) G. Garcia-Belmonte, P. P. Boix, J. Bisquert, M. Lenes, H. J. Bolink, A. La Rosa, S. Filippone and N. Martin, *J. Phys. Chem. Lett.*, 2010, **1**, 2566.

6. a) A. Tamayo, T. Kent, M. Tantitiwat, M. A. Dante, J. Rogers and T.-Q. Nguyen, *Energy Environ. Sci.*, 2009, **2**, 1180; b) A. Viterisi, F. Gispert-Guirado, J. W. Ryan and E. Palomares, *J. Mater. Chem.*, 2012, **22**, 15175.

7. B. Walker, A. B. Tamayo, X.-D. Dang, P. Zalar, J. H. Seo, A. Garcia, M. Tantiwiwat and T.-Q. Nguyen, *Adv. Funct. Mater.*, 2009, **19**, 3063.

8. J. Vogelsang, J. Brazard, T. Adachi, J. C. Bolinger and P. F. Barbara, *Angew. Chem., Int. Ed.*, 2011, **50**, 2257.

9. Here amourphous-material referes to either the amorphous fraction of donor material in the active layer or most importantly to the fraction of suposedely amorphous fullerene domains.

10. T. M. Clarke, A. Ballantyne, S. Shoaee, Y. W. Soon, W. Duffy, M. Heeney, I. McCulloch, J. Nelson and J. R. Durrant, *Adv. Mater.*, 2010, **22**, 5287.

11. a) J. Bisquert, J. M. Montero, H. J. Bolink, E. M. Barea and G. Garcia-Belmonte, *phys. stat. sol. (a)*, 2006, **203**, 3762; b) J. M. Montero and J. Bisquert, *Solid-State Electron.*, 2011, **55**, 1.

12. E. von Hauff, V. Dyakonov and J. Parisi, *Sol. Energy Mater. Sol. Cells*, 2005, **87**, 149.

13. a) D. Credgington and J. R. Durrant, *J. Phys. Chem. Lett.*, 2012, **3**, 1465; b) A. Maurano, R. Hamilton, C. G. Shuttle, A. M. Ballantyne, J. Nelson, B. O'Regan, W. M. Zhang, I. McCulloch, H. Azimi, M. Morana, C. J. Brabec and J. R. Durrant, *Adv. Mater.*, 2010, **22**, 4987; c) G. Garcia-Belmonte and J. Bisquert, *Appl. Phys. Lett.*, 2010, **96**, 113301.

14. a) C. G. Shuttle, A. Maurano, R. Hamilton, B. O'Regan, J. C. de Mello and J. R. Durrant, *Appl. Phys. Lett.*, 2008, **93**, 183501; b) C. G. Shuttle, B. O'Regan, A. M. Ballantyne, J. Nelson, D. D. C. Bradley and J. R. Durrant, *Phys. Rev. B*, 2008, **78**, 113201; c) R. Hamilton, C. G. Shuttle, B. O'Regan, T. C. Hammant, J. Nelson and J. R. Durrant, *J. Phys. Chem. Lett.*, 2010, **1**, 1432; d) F. C. Jamieson, T. Agostinelli, H. Azimi, J. Nelson and J. R. Durrant, *J. Phys. Chem. Lett.*, 2010, **1**, 3306; e) A. Maurano, R. Hamilton, C. G. Shuttle, A. M. Ballantyne, J. Nelson, B. O'Regan, W. Zhang, I. McCulloch, H. Azimi, M. Morana, C. J. Brabec and J. R. Durrant, *Adv. Mater.*, 2010, **22**, 4987; f) D. Credgington, R. Hamilton, P. Atienzar, J. Nelson and J. R. Durrant, *Adv. Funct. Mater.*, 2011, **21**, 2744; g) D. Credgington, Y. Kim, J. Labram, T. D. Anthopoulos and J. R. Durrant, *J. Phys. Chem. Lett.*, 2011, **2**, 2759; h) A. Maurano, C. C. Shuttle, R. Hamilton, A. M. Ballantyne, J. Nelson, W. Zhang, M. Heeney and J. R. Durrant, *J. Phys. Chem. C*, 2011, **115**, 5947; i) D. Credgington, F. C. Jamieson, B. Walker, N. Thuc-Quyen and J. R. Durrant, *Adv. Mater.*, 2012, **24**, 2135; j) G. F. A. Dibb, F. C. Jamieson, A. Maurano, J. Nelson and J. R. Durrant, *J. Phys. Chem. Lett.*, 2013, **4**, 803.

15. A. Sanchez-Diaz, R. Pacios, U. Munecas, T. Torres and E. Palomares, *Org. Electron.*, 2011, **12**, 329.
16. a) M. P. Eng, P. R. F. Barnes and J. R. Durrant, *J. Phys. Chem. Lett.*, 2010, **1**, 3096; b) C. G. Shuttle, R. Hamilton, J. Nelson, B. C. O'Regan and J. R. Durrant, *Adv. Funct. Mater.*, 2010, **20**, 698; c) C. G. Shuttle, R. Hamilton, B. C. O'Regan, J. Nelson and J. R. Durrant, *Proc. Natl. Acad. Sci. USA*, 2010, **107**, 16448; d) D. Spoltore, W. D. Oosterbaan, S. Khelifi, J. N. Clifford, A. Viterisi, E. Palomares, M. Burgelman, L. Lutsen, D. Vanderzande and J. Manca, *Adv. Energy. Mater.*, 2013, **3**, 466.
17. a) R. C. I. MacKenzie, T. Kirchartz, G. F. A. Dibb and J. Nelson, *J. Phys. Chem. C*, 2011, **115**, 9806; b) T. Kirchartz, B. E. Pieters, J. Kirkpatrick, U. Rau and J. Nelson, *Phys. Rev. B*, 2011, **83**, 115209.
18. T. Kirchartz and J. Nelson, *Phys. Rev. B*, 2012, **86**, 165201.